International Journal of Multiphase Flow 173 (2024) 104730

Contents lists available at ScienceDirect

International Journal of Multiphase Flow

journal homepage: www.elsevier.com/locate/ijmulflow

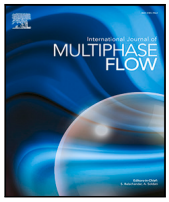

Film drainage and critical velocity of fluid particles in power-law fluids

Veronica Galantucci [a], Suat Canberk Ozan [a,b,*], Hugo Atle Jakobsen [a]

[a] Department of Chemical Engineering, Norwegian University of Science and Technology (NTNU), Trondheim, Norway
[b] SINTEF Industry, Process Technology Department, Trondheim, Norway

ARTICLE INFO

Keywords:
Coalescence
Rebound
Film drainage
Critical velocity
Non-Newtonian film
Drag force

ABSTRACT

This work studies the collision of fluid particles (bubbles or droplets) in non-Newtonian media whose viscosity obeys the power-law model, by analyzing the behavior of the drainage of the film between the particles. The model considers a time-dependent collision velocity governed by a force balance over each particle, which renders the estimation of both coalescence and rebound possible and as a result the critical velocity separating the two regimes. Results indicate that the shear-thinning behavior of the continuous medium favors coalescence, whereas shear-thickening films promote rebound. The critical velocity increases with decreasing power-law index and follows an exponential trend with the equivalent particle size for a given value of the power-law index. The exponent showing the dependency of the critical velocity on the equivalent particle size changes linearly with the power-law index within the investigated parameter range. Both the drainage behavior and the critical velocity are shown to be affected only negligibly by the selection of the drag force closure, i.e., whether they are proposed by considering Newtonian or non-Newtonian media.

1. Introduction

Dispersed flows with either bubbles or droplets distributed within a continuous medium are frequently observed in several key processes and in engineering units such as (bio)chemical reactors or separators. The optimal operation of these units requires a good insight on the interaction between the dispersed fluid particles (bubbles or droplets), including their coalescence. Although the coalescence and the interaction of fluid particles in Newtonian media has been studied extensively in the literature (see for example Liao and Lucas 2010 for an overview), the studies considering the same in non-Newtonian continuous media are far more scarce. To address this gap, this work focuses on the modeling of the collisions between fluid particles dispersed in non-Newtonian media, specifically on the coalescence and the rebound of the particles in a power-law fluid and analyzes the critical approach velocity that separates these two regimes.

The film drainage approach is one of the most well-known methods for modeling the coalescence of two fluid particles. Following the observations of Shinnar and Church (1960), this approach suggests that, the particles are brought together by the external flow field and entrap a thin film of the continuous medium in between them. For coalescence to occur, this film must drain until a critical film thickness is reached, at which the attractive intermolecular forces between the two particles become strong enough to cause rupture of the interfaces. Thus, modeling the hydrodynamics that govern the drainage of the thin film would reveal the coalescence behavior. As the thickness of this film is typically much smaller than its radius, the lubrication theory is employed in simplifying the governing equations.

The shape and the deformability of the interfaces in the film drainage models play a critical role for the accuracy of the models in replicating the experimentally observed phenomena, as well as for the complexity of the resulting model. For example, when the interfaces are not allowed to deform, whether they are spherical or spherical-caps, it is possible to solve the resulting governing equations analytically; however, the film drainage model is then not capable of estimating the formation of interfacial structures, which are known to change the coalescence time and behavior significantly (Ozan and Jakobsen, 2019a). Formation of these structures during the interaction of fluid particles has been well-documented in experiments since the observation of dimple formation by Derjaguin and Kussakov (1939). Allowing the interfaces to deform during the approach of the fluid particles on the other hand, renders the estimation of the interfacial structures possible and results in better representation of the phenomenon. However, the resulting drainage equations are then no longer analytically solvable. Further considerations on the representation of the interface in the drainage model can be summarized under two categories: the tangential mobility of the interface and the interfacial rheology, both of which are severely affected by the presence of surfactants/impurities in the dispersed system. The interfaces are often considered as rheologically ideal, i.e., they are only characterized by surface tension, yet in many real systems the presence of the impurities

* Corresponding author at: SINTEF Industry, Process Technology Department, Trondheim, Norway.
E-mail address: canberk.ozan@sintef.no (S.C. Ozan).

https://doi.org/10.1016/j.ijmultiphaseflow.2024.104730
Received 6 October 2023; Received in revised form 18 December 2023; Accepted 4 January 2024
Available online 9 January 2024

may cause the interface to exhibit viscous and viscoelastic behavior, as well as Marangoni stresses at the interface due to non-uniform surfactant distribution. All these factors impact the tangential mobility of the interface significantly. Ozan and Jakobsen analyzed the surfactant-laden systems by considering viscous (Ozan and Jakobsen, 2019b) and viscoelastic (Ozan and Jakobsen, 2020) interfaces and showed that even for relatively low amounts of impurities, the interfaces are likely to be completely immobilized depending on the values of key dimensionless parameters, such as Boussinesq, surface Peclet and surface Weissenberg numbers. Similarly, Klaseboer et al. (2000) observed that their drainage model considering immobile interfaces matched their experimental results better than the mobile model and concluded that the interfaces were immobilized in their experiments most likely due to presence of impurities.

The approach between the particles has commonly been considered to have a constant velocity (Abid and Chesters, 1994; Klaseboer et al., 2000; Bazhlekov et al., 2000; Fanebust et al., 2021) or driven by a constant interaction force (Saboni et al., 1995; Bazhlekov et al., 2000; Alexandrova, 2014) in the film drainage studies in the literature, regardless of the overall complexity of the model. Liu et al. (2019) showed that the constant approach velocity assumption is only valid when the capillary number in the system is sufficiently low, restricting the applicability of the constant velocity models to low velocity collisions. Constant interaction force assumption on the other hand, allows the approach velocity to change during the interaction of the particles, however overlooks the fact that the force arising from the pressure build-up in the film during drainage is not constant but rather a function of the shape of the interface and the film thickness. To address the discrepancy, following Manica et al. (2015)'s approach, Ozan et al. (2021) introduced a variable collision velocity in their film drainage model. The collision velocity is governed by a force balance over the fluid particles that considers buoyant, drag, and film forces (arising due to pressure build-up) and is solved simultaneously with the drainage model. Their findings indicated that the film resistance can become strong enough to reverse the approach of the fluid particles, thereby initiating the rebound process. With this approach, it is possible to estimate the outcome of a collision as rebound or coalescence within a single simulation. They further determined the critical rebound velocity, which signifies the lowest collision velocity resulting in rebound, as a function of fluid particle radii. The critical velocity separates the coalescence (low approach velocity) and rebound (high approach velocity) regimes and can be further used to model particle interactions in dispersed flow models, e.g., by employing the population balance framework (Ozan et al., 2023).

This work studies the film drainage between two fluid particles approaching each other within a non-Newtonian medium that obeys the power-law model. Fanebust et al. (2021) considered a similar setting where the collision velocities were assumed to remain constant during the interaction. Their results indicated that the coalescence time is lower for the films with stronger shear-thinning behavior and higher for the films with stronger shear-thickening behavior. The current work differs from Fanebust et al. (2021), as the collision velocity here is allowed to vary during the interaction following the force balance approach. This enables the model to estimate both rebound and coalescence outcomes, and eventually yields the critical rebound velocity for fluid particles dispersed in power-law media as a function of the fluid particle sizes, as well as the power-law model parameters. The model considers deformable, tangentially immobilized interfaces and axisymmetric collisions.

Section 2 presents the physical configuration and the film drainage model together with the closures used for determining the drag forces acting on the fluid particles moving in a power-law continuous medium. Section 3 briefly describes the numerical procedure used for the solution of the model equations. Section 4 presents and discusses the effect of the drag closures on the drainage, the changes in the drainage behavior with power-law model parameters, and the effect of the non-Newtonian behavior on the critical rebound velocity. Section 5 summarizes the conclusions of the study.

2. Physical configuration and mathematical model

The physical configuration consists of two fluid particles (bubbles or droplets) approaching each other in a non-Newtonian medium with sizes R_1 and R_2, and velocities V_1 and V_2 (Fig. 1). The fluid particles entrap a thin film of the non-Newtonian continuous phase upon their collision. The interplay between the drainage of the film and the fluid particle dynamics, e.g., the changes in the relative approach velocity V_{app}, determines the outcome of the collision as coalescence or rebound. The system can be characterized through three distinct length scales: the thickness and the radius of the deform section of the film, and the fluid particle radius (Ozan and Jakobsen, 2019a). For a gentle collision, i.e., when the deformed film radius are much smaller than the fluid particle radius, resulting in the emergence of a thin film, i.e., when the thickness of the deformed part of the film is much smaller than its radius, the particle sizes can be represented by a single equivalent radius $R_p = \frac{1}{2}\left(\frac{1}{R_1} + \frac{1}{R_2}\right)^{-1}$ (Abid and Chesters, 1994). The use of R_p and the axisymmetry assumption, simplifies the system such that modeling only one quadrant in Fig. 1 is sufficient. Thus, in this work, the drainage equations are only solved for $r \geq 0$ and $z \geq 0$. Due to the significantly different length scales emerging within the film, the lubrication theory applies within the collision zone. Then, the continuous phase mass and momentum balances read (Fanebust et al., 2021):

$$\frac{1}{r}\frac{\partial}{\partial r}\left(r v_r\right) + \frac{\partial v_z}{\partial z} = 0 \tag{1}$$

$$\frac{\partial P}{\partial r} = \frac{\partial}{\partial z}\left(\eta \frac{\partial v_r}{\partial z}\right) \tag{2}$$

and

$$\frac{\partial P}{\partial z} = 0 \tag{3}$$

where v_r and v_z are the radial and axial continuous phase velocities, P is the excess film pressure corresponding to the additional pressure generated through the interfacial deformations, and η is the non-Newtonian viscosity. At the interface, $z = h(r,t)/2$, the no-slip and the kinematic conditions respectively give:

$$v_r = U_t = 0 \tag{4}$$

$$v_z - \frac{1}{2}\frac{\partial h}{\partial r} v_r = U_n = \frac{1}{2}\frac{\partial h}{\partial t} \tag{5}$$

where U_n is the normal speed of the interface, and U_t is its tangential velocity, which is zero for immobile interfaces. Furthermore, the normal stress balance relates the interfacial stress to the continuous phase stress:

$$P = \frac{2\sigma}{R_p} - \frac{\sigma}{2r}\frac{\partial}{\partial r}\left(r\frac{\partial h}{\partial r}\right) \tag{6}$$

where σ is the surface tension. In the thin film limit, the power-law viscosity model is expressed as (Fanebust et al., 2021):

$$\eta = k\left|\frac{\partial v_r}{\partial z}\right|^{n-1} \tag{7}$$

where k is the flow consistency index and n is the flow behavior index.

Eqs. (1)–(7) are then non-dimensionalized using the following characteristic scales

$$\bar{P} = \frac{\sigma}{R_p}, \quad \bar{h} = \bar{r} = Rp, \quad \bar{v}_r = \bar{v}_z = \frac{\sigma}{\bar{\eta}}, \quad \bar{t} = \frac{R_p \bar{\eta}}{\sigma}, \quad \bar{\eta} = k^{1/n}\left(\frac{\sigma}{R_p}\right)^{1-1/n} \tag{8}$$

and manipulated analytically. The resulting equations describe the film thickness and the excess pressure in the film as a function of r and t (please refer to Chapter 2.2 of Fanebust (2021) for a detailed derivation):

$$\frac{\partial \tilde{h}}{\partial \tilde{t}} = -\frac{1}{\tilde{r}}\frac{\partial}{\partial \tilde{r}}\left[\tilde{r}\left(-\frac{\partial \tilde{P}}{\partial \tilde{r}}\right)^{1/n}\tilde{h}^{2n+1}\right]\frac{n}{(1+2n)2^{1/n+1}} \tag{9}$$

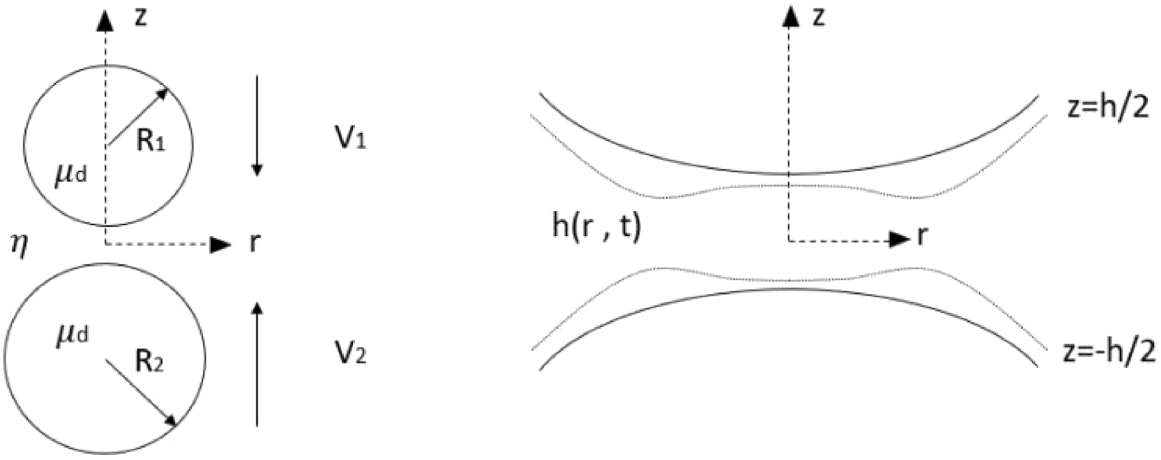

Fig. 1. Two colliding fluid particles in a non-Newtonian continuous medium and the thin film entrapped between them upon their collision.

$$\tilde{P} = 2 - \frac{1}{2\tilde{r}}\frac{\partial}{\partial \tilde{r}}\left(\tilde{r}\frac{\partial \tilde{h}}{\partial \tilde{r}}\right) + \frac{A^*}{\tilde{h}^3} \tag{10}$$

where tildes represent the dimensionless variables. The disjoining pressure is added to the normal stress balance to represent the effect of the attractive intermolecular forces between two particle interfaces (Jacob and Israelachvili, 1992). For two interfaces entrapping a thin liquid film this pressure can be expressed as $\frac{A}{6\pi h^3}$ where A is the Hamaker constant. Provided that the attractive forces are strong enough, the disjoining pressure enables the rupture of the film and estimation of coalescence. In dimensionless form, the disjoining pressure is characterized by the dimensionless Hamaker constant $A^* = \frac{A}{6\pi R_p^2 \sigma}$. Eqs. (9) and (10) are subject to boundary conditions at $\tilde{r} = 0$ following the symmetric nature of the film:

$$\left.\frac{\partial \tilde{P}}{\partial \tilde{r}}\right|_{\tilde{r}=0} = 0 = \left.\frac{\partial \tilde{h}}{\partial \tilde{r}}\right|_{\tilde{r}=0} \tag{11}$$

At $\tilde{r} = \tilde{r}_\infty$, it is assumed that the local conditions are not affected by the film dynamics, i.e., the fluid particles are locally spherical and there is no excess pressure generated, indicating that the drainage is dominated by the unidirectional bulk motion of the fluid particles along the collision axis rather than the film dynamics in the collision zone that is subject to lubrication conditions. Under these conditions the normal speed of the interface follows the relative collision velocity:

$$\tilde{P}|_{\tilde{r}=\tilde{r}_\infty} = 0 \qquad \text{and} \qquad \left.\frac{\partial \tilde{h}}{\partial \tilde{t}}\right|_{\tilde{r}=\tilde{r}_\infty} = -\tilde{V}_{app}\,(\tilde{t}) \tag{12}$$

where $V_{app} = V_2 - V_1$ is the relative approach velocity that is made dimensionless using the characteristic velocity scale presented in Eq. (8). The time dependent approach velocity of each particle is determined through a force balance over the particle (Ozan et al., 2021):

$$m_{A,i}\frac{\partial \mathbf{V}_i}{\partial t} = \mathbf{F}_{b,i} + \mathbf{F}_{d,i} + \mathbf{F}_{f,i} \tag{13}$$

where $i = 1, 2$, m is the mass of the fluid particle and $m_A = m(1 + C_m\rho_c/\rho_d)$ includes the added mass effect with the added mass coefficient C_m. The buoyant, drag, and film forces act on the particles during the collision. Here, the film force represents the resistance of the thin film to drainage and expressed as the surface integral of the excess film pressure over the particle interface. By also considering the axisymmetry, the force balance can be written as

$$m_{A,i}\frac{\partial \mathbf{V}_i}{\partial t} = m_i\left(1 - \frac{\rho_c}{\rho_d}\mathbf{g}\right) - C_{D,i}Re_i\frac{\pi}{4}\mu_c R_i \mathbf{V}_i + \mathbf{d_i} 2\pi\int_0^{r_\infty} rp\,dr \tag{14}$$

By further considering similar-sized fluid particles, i.e., $R_1 \approx R_2 \approx R_p$, the dimensionless force balance can be written as

$$\frac{\partial \tilde{V}_i}{\partial \tilde{t}} = \frac{m_i}{m_{A,i}}\frac{\mu_c^2 R_p}{\sigma^2}\left(1 - \frac{\rho_c}{\rho_d}\right)(\mathbf{g}\cdot\mathbf{k}) - Oh_{A,i}^2\left(C_{D,i}Re_i\frac{\pi}{4}\tilde{V}_i - d_i 2\pi\int_0^{\tilde{r}_\infty}\tilde{r}\tilde{p}\,d\tilde{r}\right) \tag{15}$$

where $Oh_{A,i} = \frac{\mu_c R_p}{\sqrt{m_{A,i}\sigma}}$ is the Ohnesorge number, C_D is the drag coefficient, $Re = 2R\rho_c|V|/\mu_c$ is the instantaneous Reynolds number, and $\mathbf{d}_1 = d_1\mathbf{k} = \mathbf{k}$ and $\mathbf{d}_2 = d_2\mathbf{k} = -\mathbf{k}$ are added to correctly represent the film resistance's impact on the velocities. Here $\mathbf{k}$ is a unit vector that coincides with the line of impact for the collision. Eq. (15) (and its alternative form presented in Section 2.1 for shear-thinning continuous media) is subject to the initial condition $V_{1,0} = -V_{2,0} = -V_{app,0}/2$.

2.1. Drag coefficient

A commonly accepted drag coefficient for spherical particles in Newtonian fluids is given by Schiller (1933):

$$C_{D,i} = 24Re_i^{-1}(1 + 0.15Re_i^{0.687}) \tag{16}$$

However, when the particles are in motion through a power-law fluid, alternative formulations are needed. For the shear-thinning continuous phase, Dazhi and Tanner (1985) give the drag force on a spherical particle as

$$F_d = 6\pi k\left(\frac{|V_i|}{2R_p}\right)^{n-1} V_i R_p X(n) \tag{17}$$

where $X(n)$ is a correction factor that scales with the strength of the shear-thinning behavior of the fluid. Fig. 2 shows the behavior of the correction factor as a function of n together with the fitted curve used for interpolation. Then, with the shear-thinning drag expression, the force balance becomes:

$$\frac{\partial \tilde{V}_i}{\partial \tilde{t}} = \frac{m_i}{m_{A,i}}\frac{\mu_c^2 R_p}{\sigma^2}\left(1 - \frac{\rho_c}{\rho_d}\right)(\mathbf{g}\cdot\mathbf{k}) - Oh_{A,i}^2\left(6\pi\left(\frac{|\tilde{V}_i|}{2}\right)^{n-1}|\tilde{V}_i|X(n) - d_i 2\pi\int_0^{\tilde{r}_\infty}\tilde{r}\tilde{p}\,d\tilde{r}\right) \tag{18}$$

Notice that Eq. (18) follows the same form as the force balance presented in Eq. (15), but the drag force is explicitly written without the use of C_D. Furthermore the fitted equation for $X(n)$ given in Fig. 2 should only be used for $0.5 \le n \le 1$, as it may give inaccurate estimations when extrapolated to $n < 0.5$ range. Following the approach of Dazhi and Tanner (1985), the drag coefficient can be

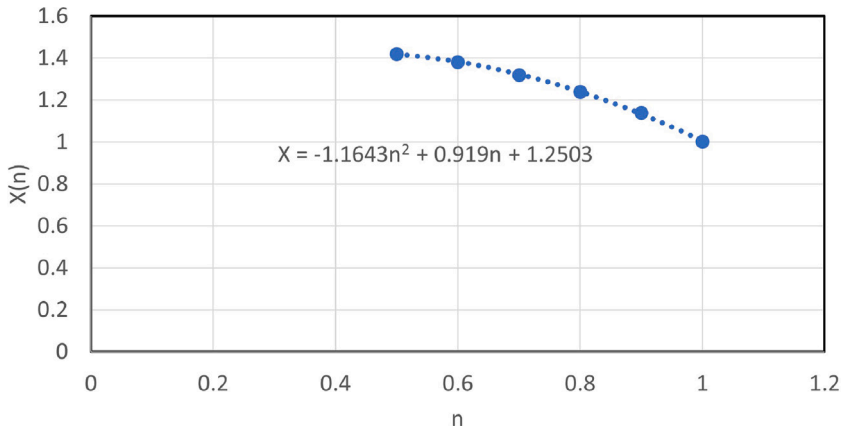

Fig. 2. The drag correction factor X as a function of n for shear-thinning fluids together with the fitted curve for interpolation. The experimental data points are taken from Dazhi and Tanner (1985).

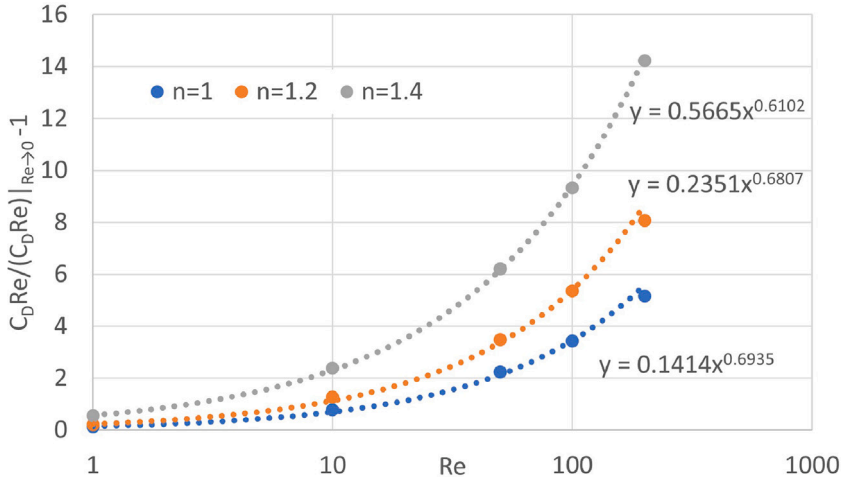

Fig. 3. Curve fitting of the drag correction factor values C_D for spheres in dilatant fluids. Curves are fitted for different n values: 1 (Newtonian case), 1.2, and 1.4. Raw data from: Tripathi and Chhabra (1995).

formulated $C_{D,shear-thinning} = C_{D,Newtonian}X(n)$, where the Newtonian drag coefficient is given by Eq. (16). The measurements for the drag on the spherical particles in shear-thickening fluids are far more scarcely available in the literature compared to the shear-thinning case. Consequently, no counterpart of Eq. (18) is available for this case. Based on the measurements of Tripathi and Chhabra (1995), the current work proposes shear-thickening drag coefficient expressions in the same form as the Schiller–Naumann expression

$$C_D = \left(\frac{C_D}{Re}\right)\Big|_{Re\to 0} Re^{-1}(1 + f(Re)). \tag{19}$$

The experimental data points of Tripathi and Chhabra (1995) are presented in Fig. 3 together with the fit results:

$$n = 1.2: \quad C_D = \frac{19.85}{Re}(1 + 0.23Re^{0.681})$$
$$n = 1.4: \quad C_D = \frac{13.67}{Re}(1 + 0.57Re^{0.610}) \tag{20}$$

For the intermediate values of n, the drag coefficient is calculated via interpolation. To better visualize the overall effect of the non-Newtonian behavior on the drag coefficient, C_D for different n is presented in Fig. 4 as a function of Re. In Fig. 4, the corresponding calculation procedure described int this section is used for each type of different rheological behavior.

Hereafter, tildes in the dimensionless variables are omitted for the sake of simplicity.

3. Numerical procedure

For the spatial discretization, a spectral scheme is used, where a purely geometric derivative matrix $[D]$ is obtained through Chebyshev polynomials that are mapped linearly to fit the domain of $r = 0$ to $r = r_\infty$ (Guo et al., 2013), whereas for the time derivatives, a second-order backward differentiation is employed. Eqs. (9) and (10) are solved simultaneously together with the boundary conditions presented in Eqs. (11) and (12). The particle velocities V_1 and V_2 are calculated via the ordinary differential equation presented in Eq. (15) (or Eq. (18) for the shear-thinning case) to determine $V_{app}(t)$, which is fed to the main solver as a boundary condition in each time step.

To determine the first $V_{app,0}$ that results in rebound, i.e., the critical rebound velocity V_c, a search algorithm is employed. The algorithm begins with an initial guess, $V_{app0,guess}$ and at each step updates the $V_{app,0}$ depending on the outcome of the film drainage model, i.e., whether the simulation resulted in coalescence or rebound. After each try, the range of the $V_{app,0}$ domain is shrunk until V_c is obtained with 0.01% accuracy for a given set of physical parameters.

4. Results and discussion

This section first discusses the influence of the non-Newtonian drag expressions (in Section 2.1) on the collisions of fluid particles in shear-thinning and shear-thickening continuous media, then analyzes the drainage and collision behaviors in relation with the strength of

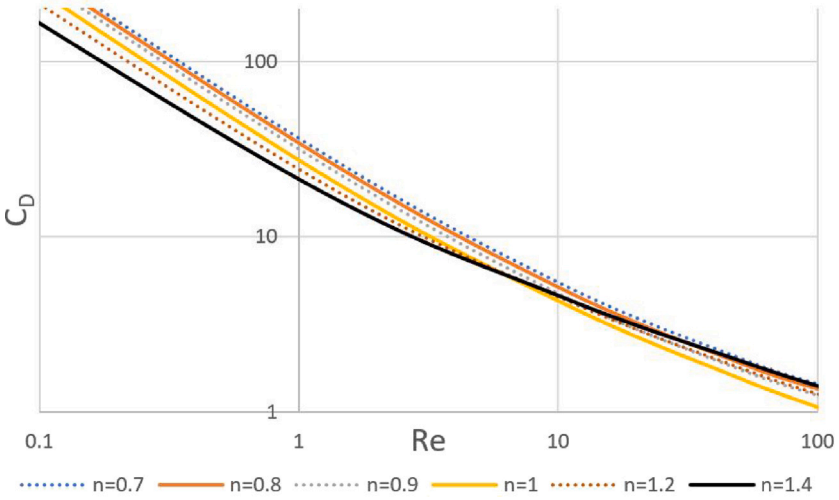

Fig. 4. Drag coefficient as a function of Re for different values of n. For each type of rheological behavior, the corresponding calculation procedure described throughout Section 2.1 is employed.

the non-Newtonian behavior of the continuous medium, and finally presents the critical rebound velocities for fluid particles dispersed in the power-law fluid. The solvers produced in this work are verified in two steps: first the implementation of the non-Newtonian drainage equations has been verified against the results of Fanebust et al. (2021) by considering a constant V_{app}, and then the correctness of the implementation of the force balance and $V_{app}(t)$ has been ensured by successfully reproducing the V_c-curves presented by Ozan et al. (2021) for $n = 1$. The physical parameters, such as dispersed phase viscosity and surface tension, are estimated by considering air bubbles dispersed in an aqueous non-Newtonian solution with properties sufficiently close to water except for the non-Newtonian viscosity behavior. Similarly, the dimensionless groups A^* and Oh_A^2 are determined for a given R_p based on air-in-water system's physical properties. In all simulations, $R_p \approx R_1 \approx R_2$ is used and the magnitude of the individual fluid particle velocities are taken equal, i.e., $V_1 = -V_2 = -V_{app}/2$.

The time dependent V_{app} allows the drainage model to inherently estimate different collision outcomes without requiring any supplementary calculations: coalescence, rebound, or steady-state. Following Ozan et al. (2021), the outcome of a collision is deemed coalescence when the minimum film thickness, h_{min} virtually goes to zero due to the strong attractive intermolecular forces dominating the system in small separation distances. The rebound stems from the film force which signifies the strength of the film's resistance to drainage. Given that the film is resistant enough, this force reverses the direction of the collision, i.e., changes the sign of V_{app}, and initiates the rebound process. However, the collision outcome is only labeled as rebound once the initial h_{min} value is recovered. Whether the rebound process began or not, it is also possible that the fluid particles reach an agglomeration-like state with a steady value of h_{min} with time, due to the drag forces acting on them. In this case, the secondary mechanisms such as disturbances in the system or fluctuations in the main flow may break the steady-state and change the collision outcome (Ozan et al., 2021). Such mechanisms are not further studied in this work and the collision outcome is deemed as steady-state. The minimum initial separation distance is taken as $h_{min,0} = 0.1$ and the initial film thickness as $h_0 = h_{min,0} + r^2$ to resemble initially spherical fluid particles. Starting the simulations from larger separation distances were shown to have no significant impact on the collision outcome and the critical rebound velocities (Ozan et al., 2021).

4.1. Effect of the non-Newtonian drag expressions

The drag expressions for spherical fluid particles dispersed in continuous media exhibiting power-law behavior are obtained in Section 2.1 based on literature data. The extent of the impact of these expressions on the film drainage behavior is tested by observing the time evolution of the minimum film thickness, h_{min}. Fig. 5 presents two h_{min} curves for each value of n, one obtained by assuming Newtonian drag behavior (Eq. (16)) and one with the corresponding non-Newtonian expression in Section 2.1. As can be seen in Fig. 5, the choice of the drag expression does not significantly affect the drainage behavior within the investigated range of the parameter space. However, the seemingly insignificant changes due to the drag expression can actually alter the outcome of the collision under the right conditions. For example, for a fluid particle couple of $R_p = 0.5$ mm colliding with $V_{app,0} = 0.0003$ within the continuous medium with $n = 0.9$ using the Schiller–Naumann drag expression estimates coalescence (as $h_{min} \to 0$), whereas the use of its non-Newtonian counterpart results in a h_{min} behavior that approaches steady-state. Although this is an important difference, the choice of the drag expression only slightly change the V_c values discussed throughout the rest of this work, and do not impact the conclusions drawn on the critical rebound velocities (please see Section 4.3 for examples of V_c curves obtained with different drag expressions).

4.2. Drainage behavior

The drainage behavior of the thin film emerging between two fluid particles upon their collision carries crucial information that helps better understand the behavior of the estimated critical rebound velocities. Fig. 6 presents film thickness profiles for $R_p = 1$ mm, $V_{app,0} = 0.0008$ (dimensionless) for different values of n at the same specific time steps obtained by using the corresponding non-Newtonian drag expressions. As can be seen, with decreasing n, the drainage rate increases and the film thickness reaches smaller values. This can also be interpreted as films of stronger shear-thinning nature resulting in easier/faster drainage, whereas the opposite is true for the shear-thickening films. This is a direct implication of the film's viscosity that scales with n following the power-law expression. This conclusion can be extended further to the collision outcomes: the ease of drainage due to lowered film viscosity under shear would help particles coalesce more easily/faster at a given $V_{app,0}$ as the value of n decreases. As the coalescence outcome is promoted by the decreasing n, the first $V_{app,0}$ at which rebound is observed is expected to be larger for larger n. Fig. 7 shows the time evolution of the minimum film thickness for $R_p = 0.5$ mm and $V_{app,0} = 0.0003$ for shear-thinning and shear-thickening films obtained by employing the corresponding non-Newtonian drag expressions. In Fig. 7(a), it is seen that stronger shear-thinning behavior leads to faster

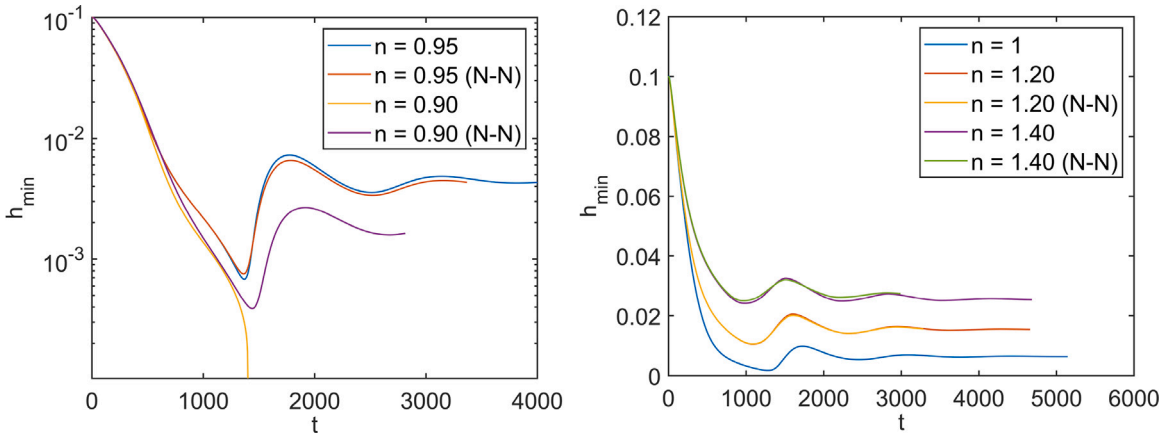

Fig. 5. Comparison of the time evolution of the minimum film thickness h_{min} obtained by using Schiller–Naumann expression (Eq. (16)) and the non-Newtonian (denoted with N-N) drag expressions. $V_{app,0} = 0.0003$ and $R_p = 0.5$ mm.

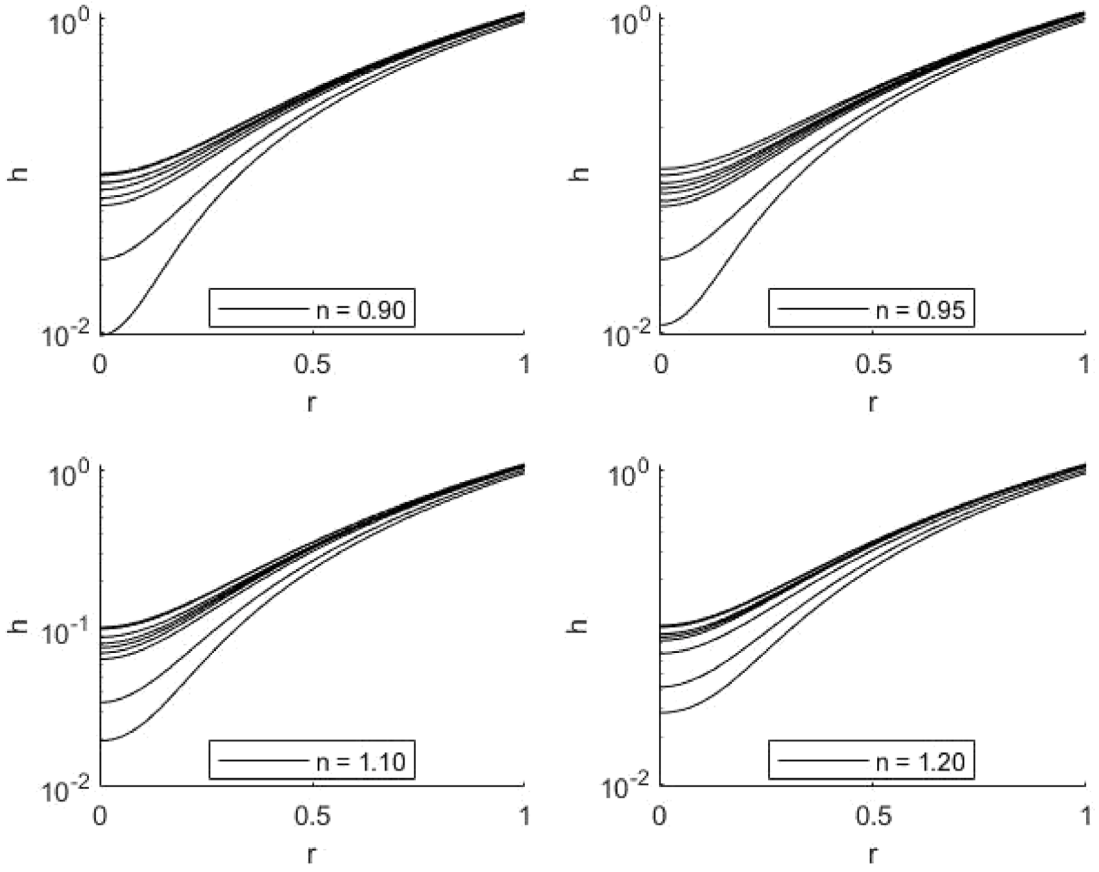

Fig. 6. Film thickness profiles as a function of n for $R_p = 1$ mm and $V_{app,0} = 0.0008$. The profiles are plotted at the same dimensionless times in all plots: t = [0, 50.6, 134.1, 273.2, 412.4, 2221, 2499, 2778].

thinning of the film, and provided that n is low enough ($n \leq 0.9$ for this specific parameter set), to coalescence. An increase in the strength of the shear-thinning behavior also results in faster coalescence times. For the shear-thickening film, on the other hand, no coalescence is observed for the particular parameter set analyzed in Fig. 7; however, it is evident that films exhibiting stronger shear-thickening properties yield larger steady h_{min} values due to the film's increased viscous resistance to drainage. It must be noted that the consistency index k, on the other hand, does not appear in the dimensionless set of equations or in the resulting dimensionless groups except for the characteristic scales. This indicates that k does not change any conclusions drawn regarding the behavior in this section and only impact the numerical values once they are considered in terms of dimensional variables.

To gain a better insight on the impact of the interfacial deformability (and of the resulting interfacial structures such as dimples) on the local dynamics on the non-Newtonian films, the dimensionless radial velocity v_r and the dimensionless viscosity η/η_0 in the film are presented in Fig. 8 for $n = 0.95$ and $n = 1.1$, where η_0 denotes the no-shear viscosity. The cut-off in the large z limit of the plots represent the position of the interface and reveals its shape, whereas the cut-off in the lower z limit is purely due to the logarithmic nature of the plot, i.e., $z = 0$ is omitted. Fig. 8 reveals that, for both shear-thinning and

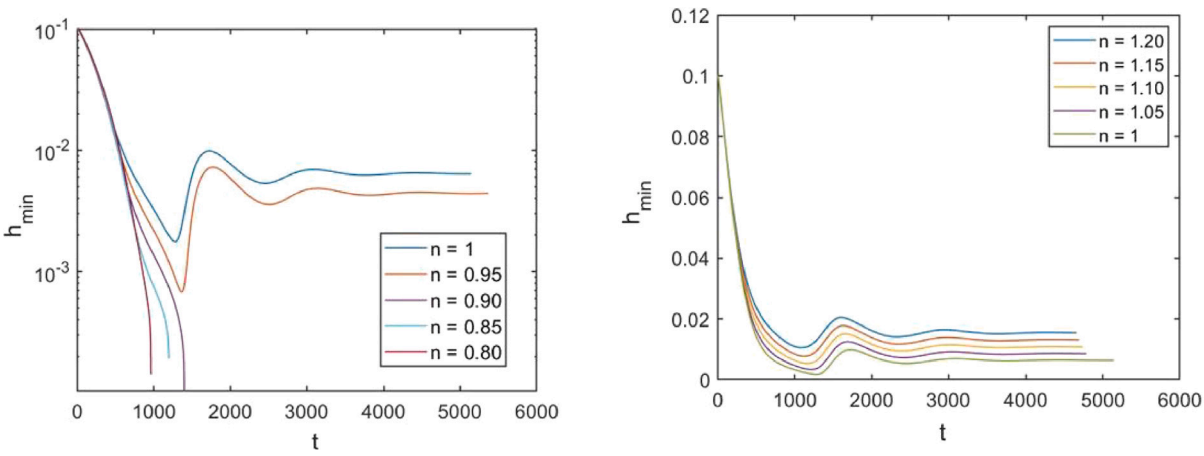

Fig. 7. Time evolution of the minimum film thickness for different n. $V_{app,0} = 0.0003$ and $R_p = 0.5$ mm.

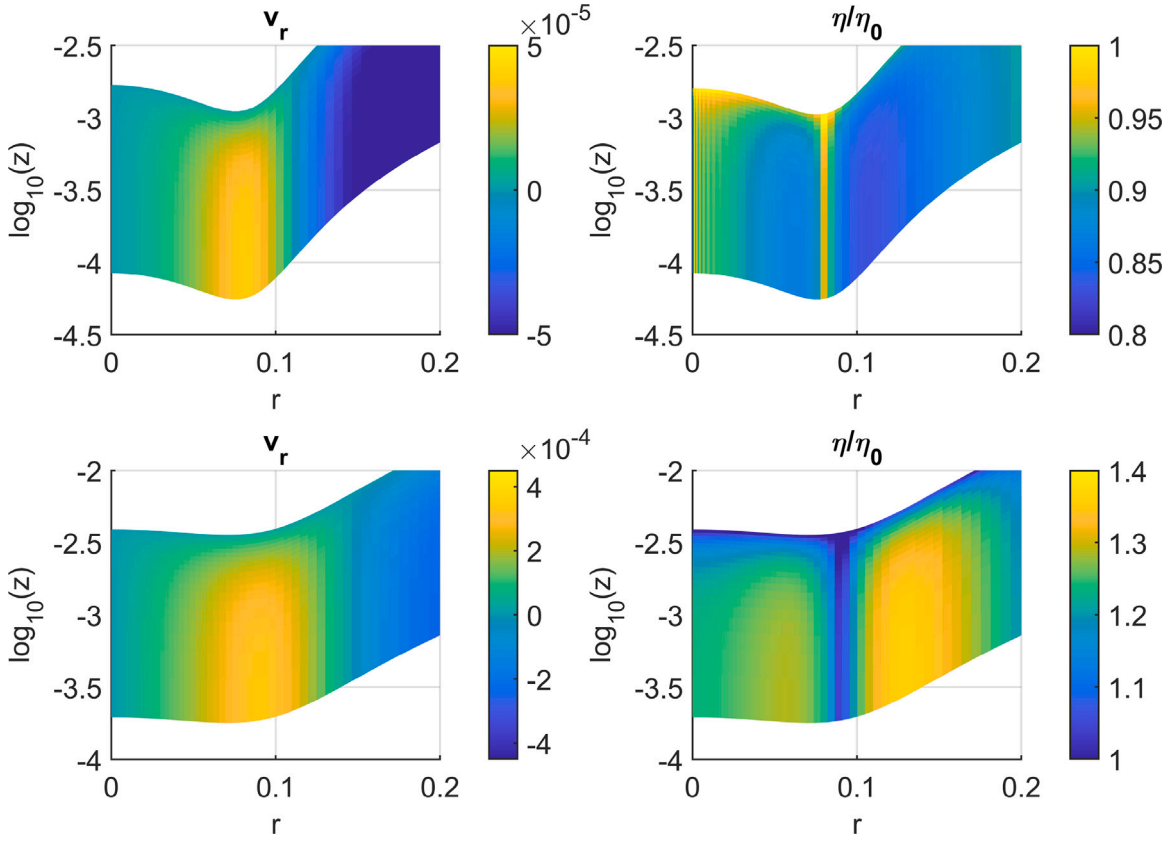

Fig. 8. Dimensionless radial velocity and viscosity for $n = 0.95$ (top) and $n = 1.1$ (bottom) inside the film. $V_{app,0} = 3.75e-4$, $R_p = 1$ mm, $t = 1062$.

shear-thickening films, the radial velocity changes the most drastically around the radial position where dimpling occurs ($r \approx 0.08$) with a plateau at the dimple position. The high shear-rate around the dimple of the film results in decreasing η for the shear-thinning film and increasing η for the shear-thickening one. As v_r plateaus around the dimple the calculated viscosity values are near the value of η_0. Similarly for $r = 0$ and $z = h/2$, respectively due to the symmetry boundary condition and the tangentially immobile interface assumptions, the viscosity approximates its value in the no-shear limit. The behavior of η around the dimpled region promotes further growth of the dimple in the shear-thinning case, whereas it limits the growth for $n > 1$. The typically large values of η for $n > 1$ slows down the film drainage, and in the opposite fashion, the low values of η for $n < 1$ enhances the drainage.

4.3. Critical rebound velocity

The smallest approach velocity, $V_{app,0}$, for which the rebound outcome is encountered, is referred to as the critical bounce velocity and represented with V_c. The critical velocity depends strongly on the physical properties of the dispersed system as well as the fluid particle sizes. In this study, as the characteristic velocity scale is a function of the power-law model parameters n and k, discussing the

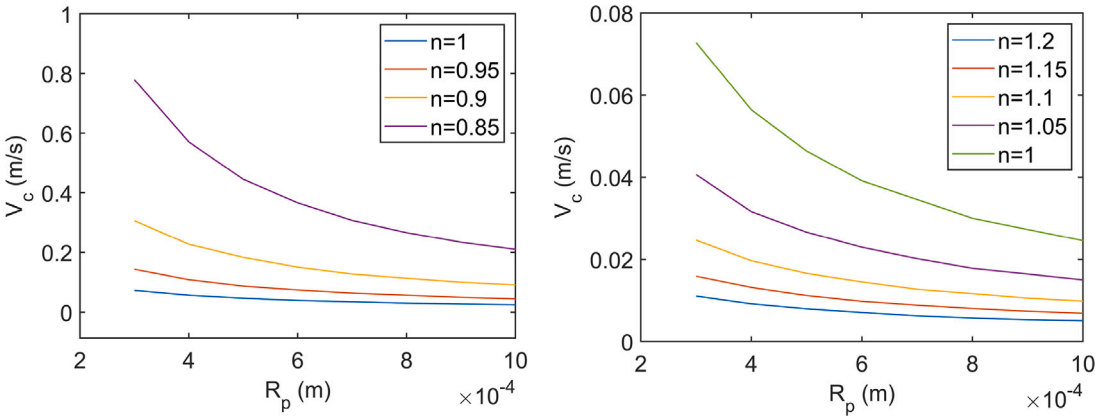

Fig. 9. Effect of the power-law index on the critical velocity for different type of fluids.

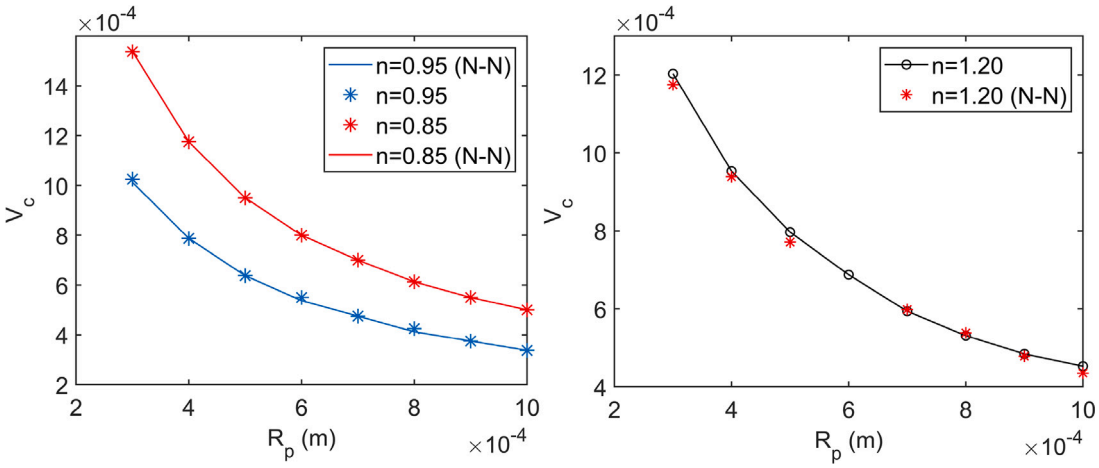

Fig. 10. Examples of dimensionless V_c curves for different n obtained with Schiller–Naumann drag expression and with the non-Newtonian (denoted with N-N) counterparts.

dimensional V_c values provides a clearer understanding of the effects of the non-Newtonian film characteristics on the critical rebound velocity. Therefore all the values presented hereafter are re-dimensionalized following:

$$V_c(m/s) = \tilde{V}_c \frac{\sigma}{k^{(1/n)} \left(\frac{\sigma}{R_p}\right)^{1-1/n}} \tag{21}$$

where k is assumed to be 1×10^{-3} Pa $\cdot s^n$ for easier comparison with the reference Newtonian case, i.e., air bubbles dispersed in water. Eq. (21) shows the effect of the critical velocity inherently without requiring any further simulations or analytical manipulations: once $\tilde{V}_c$ is determined for a given pair of R_p and n through simulation of the dimensionless equations, V_c can be calculated directly by inserting the value of k amongst the other physical parameters, σ and R_p. Fig. 9 reveals that as n increases, rebound is promoted and smaller values of V_c are obtained. This is in agreement with the findings of Section 4.2, where the drainage rate was found to be enhanced by the decreasing film viscosities for lower values of n, which in turn favors the coalescence outcome over rebound. This eventually results in a need of higher collision energies (in other words larger $V_{app,0}$) for the rebound to occur. Fig. 10 show examples of the dimensionless V_c curves obtained by employing the non-Newtonian drag expressions introduced in Section 2.1 together with the ones obtained with the Schiller–Naumann drag model. Within the investigated parameter range, the selection of the drag expression appears to have no significant impact on the resulting V_c values.

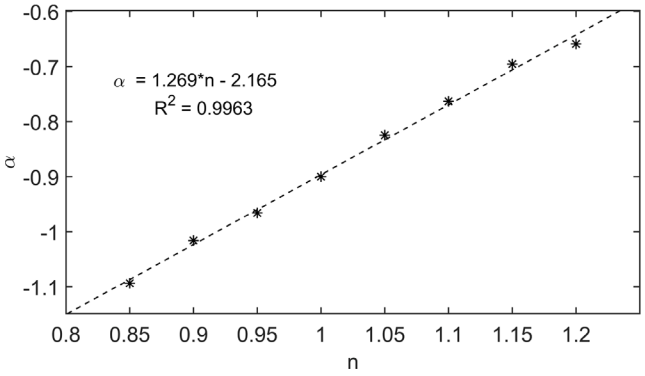

Fig. 11. Effect of the power-law index on the critical velocity for different type of fluids.

All the dimensional V_c curves presented in Fig. 9 follow an exponential trend with the equivalent particle size, in the form of $V_c = \beta R_p^{\alpha}$. Parameter fitting on these data reveals that the dependence of the exponent α on n can be approximated as linear, as shown in Fig. 11. The value of this exponent can play an important role in further studies on dispersed flows in non-Newtonian systems, as it sheds light to the particle size dependency of the critical velocity, and as a result of the coalescence behavior.

5. Conclusions

This work focuses on the interaction between the fluid particles dispersed in a non-Newtonian continuous medium whose viscosity follows the power-law model. The films exhibiting stronger shear-thinning behavior is found to promote the drainage, i.e., increase drainage rate and thereby render coalescence more likely; whereas the shear-thickening behavior promotes the rebound. This results in larger critical rebound velocities for particles colliding in shear-thinning media than those in shear-thickening media. In other words, for a given equivalent particle radius, the critical rebound velocity increases with the decreasing power-law index n. The choice between the different drag expressions, regardless of whether they are proposed considering Newtonian or non-Newtonian continuous media, is found to have negligible effect on the critical velocity values within the investigated range of n.

CRediT authorship contribution statement

Veronica Galantucci: Conceptualization, Formal analysis, Investigation, Methodology, Validation, Visualization, Writing – original draft, Writing – review & editing. **Suat Canberk Ozan:** Conceptualization, Formal analysis, Investigation, Methodology, Project administration, Software, Supervision, Validation, Visualization, Writing – original draft, Writing – review & editing. **Hugo Atle Jakobsen:** Conceptualization, Methodology, Project administration, Supervision, Writing – review & editing.

Declaration of competing interest

The authors declare that they have no known competing financial interests or personal relationships that could have appeared to influence the work reported in this paper.

Data availability

Data will be made available on request.

References

Abid, S., Chesters, A.K., 1994. The drainage and rupture of partially-mobile films between colliding drops at constant approach velocity. Int. J. Multiphase Flow 20 (3), 613–629.

Alexandrova, S., 2014. Film drainage and coalescence of drops in the presence of surfactant. J. Chem. Technol. Metall. 49 (4).

Bazhlekov, I.B., Chesters, A.K., Van de Vosse, F.N., 2000. The effect of the dispersed to continuous-phase viscosity ratio on film drainage between interacting drops. Int. J. Multiph. Flow 26 (3), 445–466.

Dazhi, G., Tanner, R.I., 1985. The drag on a sphere in a power-law fluid. J. Non-Newton. Fluid Mech. 17 (1), 1–12.

Derjaguin, B.V., Kussakov, M., 1939. Anomalous properties of thin polymolecular films. Acta Physicochim. URSS 10 (1), 25–44.

Fanebust, M., 2021. Investigation of Coalescence Through Film Drainage Modeling in Chemical-and Bioreactors with Non-Newtonian Continuous Media (Master's thesis). NTNU.

Fanebust, M., Ozan, S.C., Jakobsen, H.A., 2021. Coalescence of fluid particles with deformable interfaces in non-Newtonian media. Int. J. Multiph. Flow 144, 103787.

Guo, W., Labrosse, G., Narayanan, R., 2013. The Application of the Chebyshev-Spectral Method in Transport Phenomena. Springer Science & Business Media.

Jacob, N.I., Israelachvili, N., 1992. Intermolecular and Surface Forces. Academic, San Diego.

Klaseboer, E, Chevaillier, J Ph, Gourdon, C, Masbernat, Olivier, 2000. Film drainage between colliding drops at constant approach velocity: experiments and modeling. Journal of colloid and interface science 229 (1), 274–285.

Liao, Y., Lucas, D., 2010. A literature review on mechanisms and models for the coalescence process of fluid particles. Chem. Eng. Sci. 65 (10), 2851–2864.

Liu, B., Manica, R., Liu, Q., Klaseboer, E., Xu, Z., Xie, G., 2019. Coalescence of bubbles with mobile interfaces in water. Phys. Rev. Lett. 122 (19), 194501.

Manica, R., Klaseboer, E., Chan, D.Y., 2015. Force balance model for bubble rise, impact, and bounce from solid surfaces. Langmuir 31 (24), 6763–6772.

Ozan, S.C., Hosen, H.F., Jakobsen, H.A., 2021. On the prediction of coalescence and rebound of fluid particles: A film drainage study. Int. J. Multiph. Flow 135, 103521.

Ozan, S.C., Jakobsen, H.A., 2019a. On the effect of the approach velocity on the coalescence of fluid particles. Int. J. Multiph. Flow 119, 223–236.

Ozan, S.C., Jakobsen, H.A., 2019b. On the role of the surface rheology in film drainage between fluid particles. Int. J. Multiph. Flow 120, 103103.

Ozan, S.C., Jakobsen, H.A., 2020. Effect of surface viscoelasticity on the film drainage and the interfacial mobility. Int. J. Multiph. Flow 130, 103377.

Ozan, S.C., Solsvik, J., Jakobsen, H.A., 2023. A bubble coalescence kernel combining the characteristics of the film drainage, energy, and critical velocity models. Chem. Eng. Sci. 269, 118458.

Saboni, A., Gourdon, C., Chesters, A.K., 1995. Drainage and rupture of partially mobile films during coalescence in liquid-liquid systems under a constant interaction force. J. Colloid Interface Sci. 175 (1), 27–35.

Schiller, V.L., 1933. Uber die grundlegenden Berechnungen bei der Schwerkraftaufbereitung. Z. Vereines Deutscher Inge. 77, 318–321.

Shinnar, R., Church, J.M., 1960. Statistical theories of turbulence in predicting particle size in agitated dispersions. Ind. Eng. Chem. 52 (3), 253–256.

Tripathi, A., Chhabra, R.P., 1995. Drag on spheroidal particles in dilatant fluids. AIChE J. 41 (3), 728–731.